



Use of CALIPSO lidar observations to evaluate the cloudiness simulated by a climate model

H. Chepfer,¹ S. Bony,¹ D. Winker,² M. Chiriaco,³ J.-L. Dufresne,¹ and G. Sèze¹

Received 2 April 2008; revised 22 May 2008; accepted 16 June 2008; published 5 August 2008.

[1] New space-borne active sensors make it possible to observe the three-dimensional structure of clouds. Here we use CALIPSO lidar observations together with a lidar simulator to evaluate the cloudiness simulated by a climate model: modeled atmospheric profiles are converted to an ensemble of subgrid-scale attenuated backscatter lidar signals from which a cloud fraction is derived. Except in regions of persistent thick upper-level clouds, the cloud fraction diagnosed through this procedure is close to that actually predicted by the model. A fractional cloudiness is diagnosed consistently from CALIPSO data at a spatio-temporal resolution comparable to that of the model. The comparison of the model's cloudiness with CALIPSO data reveals discrepancies more pronounced than in previous model evaluations based on passive observations. This suggests that space-borne lidar observations constitute a powerful tool for the evaluation of clouds in large-scale models, including marine boundary-layer clouds.
Citation: Chepfer, H., S. Bony, D. Winker, M. Chiriaco, J.-L. Dufresne, and G. Sèze (2008), Use of CALIPSO lidar observations to evaluate the cloudiness simulated by a climate model, *Geophys. Res. Lett.*, 35, L15704, doi:10.1029/2008GL034207.

1. Introduction

[2] Clouds are the primary modulators of the Earth's radiation budget and still constitute the main source of uncertainty in model estimates of climate sensitivity [Randall *et al.*, 2007]. Clouds simulated by climate models have long been evaluated using passive remote-sensing [e.g., Zhang *et al.*, 2005], making the vertical structure of clouds difficult to assess. With the new generation of satellites carrying cloud profiling radar and lidar instruments such as CloudSat [Stephens *et al.*, 2002], ICESat/GLAS [Spinhirne *et al.*, 2005] and CALIOP/CALIPSO [Winker *et al.*, 2007] a near-global view of the three-dimensional distribution of clouds becomes possible. However, to make the comparison between modeled clouds and these observations meaningful, it is necessary to take into account the effects of cloud overlap, spatial resolution, and active signal attenuation.

[3] For this purpose, we propose a methodology of comparison of CALIOP/CALIPSO lidar data with modeled clouds that is intermediate between “model-to-satellite” [Morcrette, 1991; Doutriaux-Boucher *et al.*, 1998; Chiriaco

et al., 2006; Chepfer *et al.*, 2007] and “satellite-to-model” approaches: grid-scale model outputs are converted to an ensemble of subgrid-scale lidar signals while high-resolution CALIPSO lidar signals are averaged to the model vertical resolution, and then a cloud fraction is diagnosed from these signals similarly for model and for observations.

[4] The lidar simulator is described in Section 2, the processing of CALIPSO data is presented in Section 3 and the cloud detection method in Section 4. The methodology of model-data comparison is then applied to the general circulation model (GCM) LMDZ4 [Hourdin *et al.*, 2006], and the results are presented in Section 5.

2. Simulation of Lidar Profiles From Climate Model Outputs

2.1. Lidar Equation

[5] Our aim is to diagnose from climate model outputs the lidar profiles that would be observed by CALIPSO if the satellite was flying above an atmosphere similar to that predicted by the model. At the wavelength of the CALIOP/CALIPSO lidar ($\lambda = 532$ nm), atmospheric cloud particles and gas molecules contribute to scattering but not to absorption. In these conditions, the lidar Attenuated Backscattered (ATB) signal corrected of geometrical effects and normalized to the molecular signal is given by:

$$ATB(z) = (\beta_{sca,part}(z) + \beta_{sca,mol}(z)) \cdot e^{-2\eta \int_{zTOA}^z (\alpha_{sca,part}(z) + \alpha_{sca,mol}(z)) \cdot dz} \quad (1)$$

where $\beta_{sca,part}$, $\beta_{sca,mol}$ are lidar backscatter coefficients [$m^{-1}sr^{-1}$] and $\alpha_{sca,part}$, $\alpha_{sca,mol}$ attenuation coefficients [m^{-1}] for particles and molecules, and η is a multiple scattering coefficient [Chiriaco *et al.*, 2006].

[6] The molecular properties ($\beta_{sca,mol}$ and $\alpha_{sca,mol}$) are computed from Collis and Russel [1976] as a function of temperature and pressure. The particle backscattered coefficient $\beta_{sca,part}$ is linked to the attenuation coefficient $\alpha_{sca,part}$ and the backscatter-to-extinction ratio k_{part} [sr^{-1}] through:

$$\beta_{sca,part}(z) = k_{part}(z) \cdot \alpha_{sca,part}(z) \quad (2)$$

$$\alpha_{sca,part}(z) = \int \pi r^2 Q(r) n(r, z) dr \quad (3)$$

and $k_{part} = P(\pi)/4\pi$, where r is the particle radius, $n(r, z)$ the particle size distribution, $P(\pi)$ the backscattering phase function and $Q(r)$ the scattering efficiency. To be consistent with the GCM, we assume that the cloud particles are spherical. Therefore, $P(\pi)$ is parameterized as a function of

¹LMD/IPSL, CNRS, Université Pierre et Marie Curie, Paris, France.

²NASA/LaRC, Hampton, Virginia, USA.

³SA/IPSL, CNRS, Université Versailles-Saint Quentin, Paris, France.

the effective radius using Mie theory and, as most of the cloud particles are larger than $\lambda = 532$ nm, $Q(r)$ is set to 2.

[7] The multiple scattering coefficient (η) is variable in space and time as a function of the lidar footprint diameter, and the size, shape and density of the particles in the atmosphere. Theoretically it ranges between 0 and 1, but for CALIOP it is about 0.7 in ice clouds and less in water clouds [Winker, 2003]. Here we use $\eta = 0.7$ and check the sensitivity of the results to this value in section 5.

[8] To highlight the contribution of particles to the lidar signal, it is common to consider the scattering ratio $SR(z)$, defined as the ratio of the total ATB signal (Equation 1) over the molecular ATB signal (which is the ATB signal in the absence of particles, i.e., when $\alpha_{sca,part}(z) = 0$). $SR(z)$ is equal to 1 in the absence of particles (gas molecules only) and, when the lidar signal is not attenuated, is greater than unity in the presence of particles.

2.2. Application to GCM Outputs

[9] The LMDZ4 GCM has a horizontal resolution of 2.5° in latitude, 3.75° in longitude, and is discretized into 19 vertical levels [Hourdin *et al.*, 2006]. In each gridbox, the model calculates the vertical profiles of temperature, pressure, cloud fraction (assuming a maximum-random overlap), cloud condensate and effective radius of cloud droplets and ice crystals. These profiles are converted to an ensemble of subgrid-scale profiles by dividing each gridbox into 50 subcolumns generated stochastically using the Subgrid Cloud Overlap Profile Sampler [Klein and Jakob, 1999; Webb *et al.*, 2001]: in each subcolumn, the cloud fraction is assigned to be 0 or 1 at every model level, with the constraint that the cloud condensate and cloud fraction averaged over all subcolumns is consistent with the grid-averaged model diagnostics and the cloud overlap model assumption.

[10] In each subcolumn, the particle backscatter coefficient $\beta_{sca,part}$ and the attenuation coefficient $\alpha_{sca,part}$ are the sums of liquid and ice cloud particles coefficients (aerosols are not considered in this study). They are computed from equations (2) and (3) after the model mixing ratios of in-cloud liquid and ice water content have been converted to particle concentrations. This is done by assuming that the cloud particles are spherical with a radius equal to the effective radius predicted by the model. Finally, equation (1) is used to compute in each subcolumn of each gridbox the molecular and total ATB lidar profiles, and hence the SR profile.

3. CALIPSO Observations

[11] The CALIOP lidar, that operates at 532 and 1064 nm, was launched in April 2006 on-board the helio-synchronous CALIPSO platform [Winker *et al.*, 2007]. This study uses the total ATB measurements derived from the Version 1.10 Level 1 CALIOP dataset collected at 532 nm during night time from January to March 2007. The horizontal and vertical resolutions of these measurements are 333 m (333 m along track and 75 m cross track) and 30 m (respectively) below 8 km, and 1 km and 60 m at higher altitudes.

[12] At each time and location, a molecular ATB profile is computed by using GMAO (Global Modeling and Assimilation Office) temperature and pressure profiles [Bey *et*

al., 2001]. This profile is normalized (scaled) so as to match the Level 1 ATB profile measured between 27 and 29 km, where the atmosphere is free of particles, and then the scattering ratio (SR) is inferred by dividing the measured ATB profile by this molecular profile.

[13] Then, we reduce the vertical resolution of the CALIOP ATB profiles to that of the GCM (19 pressure levels) by vertical averaging. This makes the vertical resolution of CALIPSO profiles consistent with that of model computations and strongly increases the signal-to-noise ratio of the lidar signals (section 4 and auxiliary material).¹

4. Cloud Diagnostics

[14] The presence of cloud layers is then diagnosed consistently for the model and for observations from the vertical profile of lidar SR. For each CALIOP/CALIPSO profile or model subcolumn, we use different SR thresholds to label each atmospheric layer as “clear” (if $0.01 < SR \leq 1.2$), “cloudy” (if $SR \geq 3$ - that corresponds typically to a cloud optical depth >0.015 - or if the layer is the first fully attenuated layer encountered from top), “unclassified” (if $1.2 < SR < 3$) or “fully attenuated” (if $SR \leq 0.01$). The latest flag is set when optically thick clouds occurring in upper layers obscure the layers below and fully attenuate the laser beam.

[15] The main cloud layers (which are associated with the largest SR values in the full resolution CALIOP profile) are detected by applying these thresholds to the vertically averaged CALIOP profile, but the optically thin cloud layers such as subvisible cirrus clouds and potentially some semi-transparent clouds can be labelled as “unclassified” (auxiliary material). This illustrates that the detection of a cloud layer obviously depends on the criteria used for this detection. Advanced algorithms of cloud fraction retrieval such as those used for level 2 CALIOP products would provide a better detection of the different cloud layers (especially of the optically thinnest and subvisible ones) and thus would likely report larger cloud fractions than our simple detection method. Although this is not critical for this model-data comparison study because the cloud layers are diagnosed similarly in the model and in observations, this implies that our study ignores the optically thinnest cloud layers which may not be detected (in simulations like in observations) by our simple cloud detection criteria. Then, a “lidar-derived cloud fraction” is computed for each vertical level at the resolution of the model grid-box as the ratio of the number of “cloudy” layers (or profiles) encountered within this grid-box over the total number of layers that are not “fully attenuated”. Layered cloud fractions are also computed for three atmospheric layers: upper levels (between the 50 and 440 hPa pressure levels), middle levels (between 440 and 680 hPa) and low levels (altitudes below the 680 hPa level).

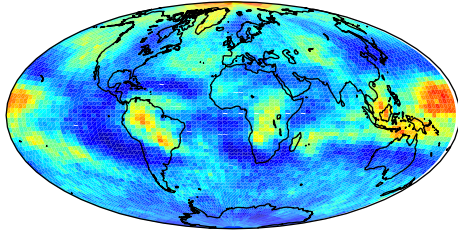
5. Results

5.1. Model Cloud Fractions Diagnosed From the Lidar Simulator

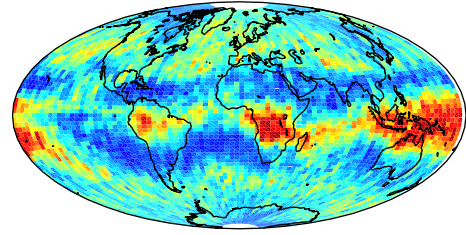
[16] The lidar simulator described in section 2 is applied to daily atmospheric profiles derived from a LMDZ4

¹Auxiliary material is available at <ftp://ftp.agu.org/apend/gl/2008GL034207>.

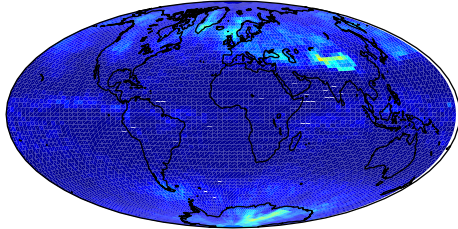
(a) HIGH CLOUDS : GCM + LIDAR SIMULATOR



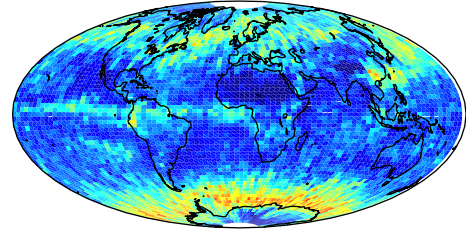
(b) HIGH CLOUDS CALIOP



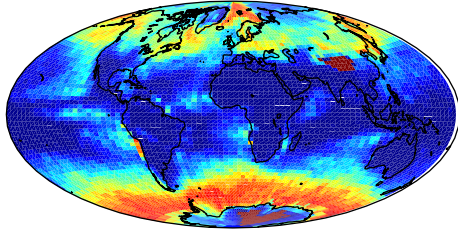
(c) MID CLOUDS : GCM + LIDAR SIMULATOR



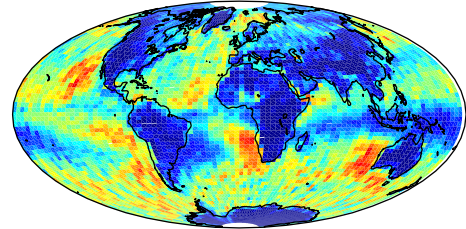
(d) MID CLOUDS CALIOP



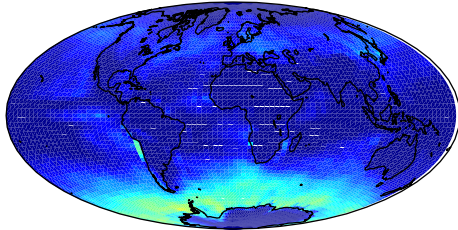
(e) LOW CLOUDS : GCM + LIDAR SIMULATOR



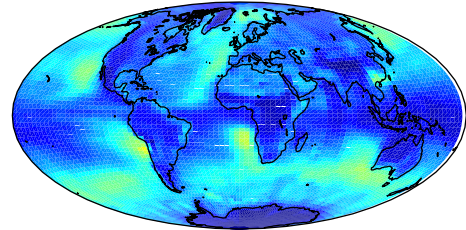
(f) LOW CLOUDS CALIOP



(g) LOW CLOUDS: GCM + ISCCP SIMULATOR



(h) LOW CLOUDS ISCCP



(i) LOW CLOUDS GCM

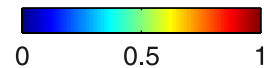
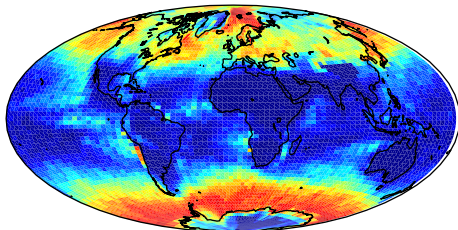


Figure 1. (a) and (b) Upper-level, (c) and (d) middle-level, and (e) and (f) low layered cloud fractions averaged for the January-February-March season. The cloud fractions derived (left) from the lidar simulator and (right) from CALIOP/CALIPSO observations are diagnosed consistently by using similar criteria. Also reported at the bottom is (h) the low-level cloud fraction derived from ISCCP-D2 data, (g) that diagnosed from the ISCCP simulator, and (i) actually predicted by the GCM.

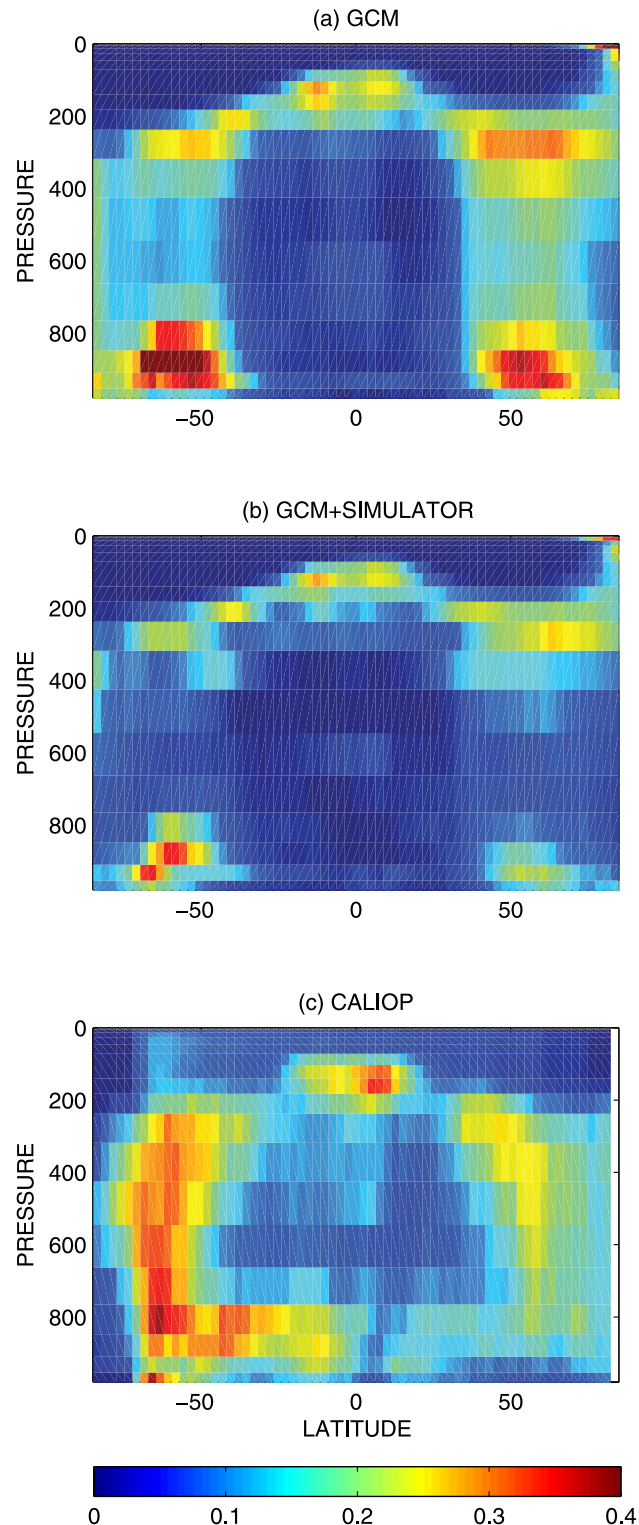


Figure 2. Vertical distribution of the zonally averaged cloud fraction for January-February-March: (a) original cloud fraction predicted by the GCM, (b) GCM cloud fraction diagnosed from the lidar simulator, and (c) cloud fraction derived from CALIOP/CALIPSO data.

simulation forced by observed sea surface temperatures. The daily cloud fractions diagnosed from the simulator are then averaged in time to produce a monthly-mean CALIPSO-like cloud fraction.

[17] Sensitivity calculations indicate that the frequency of the model inputs and simulator calculations (once a day, every 3 hour, 1.5 hour or 30 min), as well as the value of the multiple scattering coefficient assumed in the simulator (e.g., using $\eta = 0.3$ instead of $\eta = 0.7$) have negligible impacts (less than 1%) on the monthly mean CALIPSO-like cloud fraction (not shown). Using a different threshold (e.g., $SR \geq 5$ instead of $SR \geq 3$) does not change drastically the results either, which suggests that the model does not simulate many optically thin clouds.

[18] The layered cloud fractions derived from the lidar simulator and the simple cloud detection method are first compared to the cloud fractions originally predicted by the GCM. The CALIPSO-like cloud fractions (Figure 1e) are generally close to their original counterpart (Figures 1i). Since the attenuation of the backscattered lidar signal at a given height depends on the presence of overlapping clouds at higher altitudes, such a result is expected at upper levels but not necessarily at lower levels. As shown by zonal means (Figures 2a–2b), the original and CALIPSO-like cloud fractions at low and middle-levels differ mainly in regions of persistent convective activity (such as in the inter-tropical and southern-pacific convergence zones and over the warm pool) and in extratropical regions associated with frontal cloudiness. However, over a large fraction of the Earth, the simulated upper-level clouds are either not optically thick enough (the laser is typically attenuated when the optical depth is larger than 3) or not frequent or not persistent enough to obscure the view of low atmospheric layers from above. Despite the lidar attenuation effects, the CALIPSO simulator thus constitutes a powerful tool to diagnose and then to evaluate the different cloud types predicted by the GCM, including marine boundary layer clouds.

[19] Before the era of space-borne active remote sensing, GCM clouds were evaluated mostly against passive observations using the International Cloud Climatology Project (ISCCP) simulator [Klein and Jakob, 1999; Webb et al., 2001; Zhang et al., 2005]. When applied to our GCM, the ISCCP and CALIPSO simulators both diagnose an upper-level cloud fraction that resembles that originally predicted by the GCM (not shown). However, the low-level cloud fraction diagnosed from the CALIPSO simulator (Figure 1e) is much closer to that predicted by the GCM (Figure 1i) than that derived from the ISCCP simulator (Figures 1g).

5.2. Cloud Fractions Derived From CALIPSO Observations

[20] The layered and zonal mean vertical distributions of the cloud cover diagnosed from CALIPSO data using the methodology discussed in sections 3 and 4 are shown in Figures 1b, 1d, 1f, and 2c, respectively. As expected for the January-February-March season, the upper level cloud fraction exhibits maxima in deep convective regions located over tropical land areas, over the maritime continent and the pacific warm pool and over the southern-pacific convergence zone. Secondary maxima occur at extra-tropical latitudes. Middle-level clouds occur in middle-latitudes

and in regions of deep convection. CALIPSO data suggest that low-level clouds occur nearly everywhere over ocean. Maximum low-level cloud fractions are found at subtropical latitudes, at the eastern side of the ocean basins which are known to be covered by stratus and stratocumulus clouds, but cloud fractions of 40 to 60% are also reported over the tropical trade winds and at middle latitudes. Note that owing to the pronounced diurnal cycle of oceanic tropical low clouds [Rozendaal *et al.*, 1995], these nighttime values might be higher than daytime or diurnally averaged values.

[21] Sensitivity tests using the CALIPSO lidar color ratio to detect the presence of aerosols (defined as cases where the ratio between the ATB measured at 1064 and 532 nm exceeds 0.6 [Liu *et al.*, 2005]) show that the cloud detection criteria defined in section 4 do not misinterpret the presence of aerosols as low-level clouds: atmospheric layers with large aerosol burden, such as over Africa or over ocean regions west of the Sahara, are labelled as “unclassified”. On the other hand, other tests show that the cloud fraction reported in the trades critically depends on the SR threshold used for cloud detection (e.g., it is substantially reduced when the threshold is changed from 3 to 5), while it is not the case at the eastern side of the ocean basins or in the extratropics. This suggests that the large cloud fractions reported in the trades are related to the ability of lidar measurements to detect optically thin or small broken clouds owing both to their high horizontal resolution and to their high sensitivity to the presence of cloud particles. This is corroborated by the cloud fractions derived from ICESat/GLAS lidar measurements (level 2 dataset, GLA09, release 26 [Palm *et al.*, 2002]) on October and November 2003 which are of same order of magnitude as those derived from CALIPSO at the same season (not shown). The difficulty of detecting thin or/and broken low-level clouds with passive remote sensing [Turner *et al.*, 2007] presumably explains why data from the International Cloud Climatology Project (ISCCP) [Rossow and Schiffer, 1999] report substantially smaller low-level cloud fractions (Figure 1h).

5.3. Evaluation of the GCM Cloudiness Against CALIPSO Observations

[22] The comparison of the cloud fraction derived from the lidar simulator with that derived from CALIPSO observations reveals large biases in the cloudiness simulated by the GCM (Figures 1 and 2). The upper-level cloud fraction is underestimated by several tens of % in the tropical deep convective regions and the middle-level cloudiness is systematically underestimated, especially in the inter-tropical convergence zone (ITCZ) and in middle-latitude regions associated with frontal clouds. But the largest biases appear for the low-level cloud fraction, which is strongly overestimated (by about 25%) over mid-latitude oceans and is strongly underestimated (by up to a factor of 4) in the subtropics, both over the cold waters at the eastern side of the Pacific, Atlantic and Indian oceans, and offshore over the subtropical oceans. Except in mid-latitudes and in the ITCZ, these biases are unlikely to result from the attenuation of the lidar signal by overlapping optically thick clouds (section 5.1).

[23] Both in the tropics and in middle latitudes, the model-data discrepancies revealed by this comparison are

more pronounced than in previous comparisons using ISCCP observations and the ISCCP simulator (Figure 1). This suggests that using space-borne lidar observations to evaluate large-scale models will help to point out systematic biases in the cloudiness predicted by the models, especially in the simulation of marine boundary-layer clouds.

6. Conclusion

[24] This paper proposes a methodology to evaluate the cloud fraction simulated by a GCM using space borne lidar observations: on the one hand, the atmospheric profiles predicted by the GCM are converted (through a lidar simulator) to an ensemble of subgrid-scale lidar signals similar to those observed from space; on the other hand, the high vertical resolution of the lidar profiles measured by CALIOP/CALIPSO is degraded down to the vertical resolution of the GCM; then, a fractional cloudiness is diagnosed from the simulated or observed profiles of lidar scattering ratio using simple and consistent criteria.

[25] When applied to the LMDZ4 GCM, the CALIPSO-like cloud fraction derived from this methodology reproduces well the cloudiness originally predicted by the model, and this despite the attenuation effect of the lidar signal and whatever the assumed value of the multiple scattering coefficient. When applied to CALIPSO data, this simple methodology efficiently detects the main cloud layers, does not misinterpret them with the presence of aerosols, and provides cloud fraction estimates that are of same order of magnitude than those derived from the IceSAT/GLAS level 2 dataset.

[26] The comparison of the cloud fraction derived from the lidar simulator with that derived from CALIPSO data reveals large biases in the GCM cloudiness, which are more dramatic than those pointed out previously using passive observations. In particular, striking differences between GCM and CALIPSO observations (found for all seasons, not shown) occur for the marine boundary-layer clouds observed over most of the subtropical oceans. As the response of these clouds to climate change constitutes a key uncertainty for GCM estimates of climate sensitivity [Bony and Dufresne, 2005], it is of great importance to improve their representation in climate models. Efforts to improve the parameterization of shallow clouds in LMDZ4 are under way [Rio and Hourdin, 2008], and the methodology presented in this paper will allow us to quantify the extent to which the simulated cloud fraction is improved at the large scale.

[27] This study thus shows the large potential of CALIPSO observations and of the lidar simulator for the evaluation of clouds simulated by climate models. Within the framework of the Cloud Feedback Model Intercomparison Project (CFMIP, <http://www.cfmip.net>), the lidar simulator will be applied to several other climate models to examine inter-model differences and systematic biases in the simulation of clouds by GCMs.

[28] **Acknowledgments.** The authors thank Vincent Noel for fruitful discussions and for his help in the processing of CALIOP level 1 data, and to Ionela Musat for her help in GCM data processing. NASA, CNES, ICARE and Climserv are acknowledged for giving access to the CALIOP/CALIPSO data. Constructive comments from two anonymous reviewers greatly helped to improve the manuscript.

References

- Bey, I., D. J. Jacob, R. M. Yantosca, J. A. Logan, B. D. Field, A. M. Fiore, Q. Li, H. Y. Liu, L. J. Mickley, and M. G. Schultz (2001), Global modeling of tropospheric chemistry with assimilated meteorology: Model description and evaluation, *J. Geophys. Res.*, *106*, 23,073–23,095.
- Bony, S., and J.-L. Dufresne (2005), Marine boundary layer clouds at the heart of tropical cloud feedback uncertainties in climate models, *Geophys. Res. Lett.*, *32*, L20806, doi:10.1029/2005GL023851.
- Chepfer, H., M. Chiriaco, R. Vautard, and J. Spinhirne (2007), Evaluation of the ability of MM5 meso-scale model to reproduce optically thin clouds over Europe in fall using ICE/SAT lidar space-borne observations, *Mon. Weather Rev.*, *135*, 2737–2753.
- Chiriaco, M., R. Vautard, H. Chepfer, M. Haefelin, Y. Wanherdrick, Y. Morille, A. Protat, J. Dudhia, and C. F. Mass (2006), The ability of MM5 to simulate thin ice clouds: Systematic comparisons with lidar/radar and fluxes measurements, *Mon. Weather Rev.*, *134*, 897–918.
- Collis, R. T., and P. B. Russel (1976), *Laser Monitoring of the Atmosphere*, Springer, New York.
- Doutriaux-Boucher, M., J. Pelon, V. Trouillet, G. Sèze, H. Le Treut, P. Flamant, and M. Desbois (1998), Simulation of satellite lidar and radiometer retrievals of a GCM three-dimensional cloud dataset, *J. Geophys. Res.*, *103*, 26,025–26,039.
- Hourdin, F., et al. (2006), The LMDZ general circulation model: Climate performance and sensitivity to parameterized physics with emphasis on tropical convection, *Clim. Dyn.*, *19*, 3445–3482, doi:10.1007/s00382-006-0158-0.
- Klein, S. A., and C. Jakob (1999), Validation and sensitivities of frontal clouds simulated by the ECMWF model, *Mon. Weather Rev.*, *127*, 2514–2531.
- Liu, Z., A. H. Omar, Y. Hu, M. A. Vaughan, and D. M. Winker (2005), CALIOP algorithm theoretical basis document, Part 3: Scene classification algorithms, *PC-SCI-202*, NASA Langley Res. Cent., Hampton, Va.
- Morcrette, J. J. (1991), Evaluation of model-generated cloudiness: Satellite-observed and model-generated diurnal variability of brightness temperature, *Mon. Weather Rev.*, *119*, 1205–1224.
- Palm, S., W. Hart, and D. Hlavka (2002), GLAS atmospheric data products: GLAS algorithms theoretical basis document, version 4.2, Sci. Syst. Appl., Inc., Lanham, Md.
- Randall, D. A., et al. (2007), Climate models and their evaluation, in *Climate Change 2007: The Physical Science Basis. Contribution of Working Group I to the Fourth Assessment Report of the Intergovernmental Panel of Climate Change*, edited by S. Solomon et al., Cambridge Univ. Press, Cambridge, U. K.
- Rio, C., and F. Hourdin (2008), A thermal plume model for the convective boundary layer: Representation of cumulus clouds, *J. Atmos. Sci.*, *65*, 407–425.
- Rossow, W. B., and R. A. Schiffer (1999), Advances in understanding clouds from the ISCCP, *Bull. Am. Meteorol. Soc.*, *80*, 2261–2287.
- Rozendaal, M., C. Leovy, and S. Klein (1995), An observational study of diurnal variations of marine stratiform cloud, *J. Clim.*, *8*, 1795–1809.
- Spinhirne, J. D., S. P. Palm, W. Hart, D. Hlavka, and E. J. Welton (2005), Cloud and aerosol measurements from the GLAS: Overview and initial results, *Geophys. Res. Lett.*, *32*, L22S03, doi:10.1029/2005GL023507.
- Stephens, G. L., et al. (2002), The CloudSat mission and the A-train, *Bull. Am. Meteorol. Soc.*, *83*, 1771–1790.
- Turner, D. D., et al. (2007), Thin liquid water clouds: Their importance and our challenge, *Bull. Am. Meteorol. Soc.*, *88*, 177–190.
- Webb, M., C. Senior, S. Bony, and J.-J. Morcrette (2001), Combining ERBE and ISCCP data to assess clouds in three climate models, *Clim. Dyn.*, *17*, 905–922.
- Winker, D. (2003), Accounting for multiple scattering in retrievals from space lidar, in *Lidar Multiple Scattering Experiments, Proc. SPIE Int. Soc. Opt. Eng.*, *5059*, 128–139.
- Winker, D., W. Hunt, and M. McGill (2007), Initial performance assessment of CALIOP, *Geophys. Res. Lett.*, *34*, L19803, doi:10.1029/2007GL030135.
- Zhang, M. H., et al. (2005), Comparing clouds and their seasonal variations in 10 atmospheric general circulation models with satellite measurements, *J. Geophys. Res.*, *110*, D15S02, doi:10.1029/2004JD005021.

S. Bony, H. Chepfer, J.-L. Dufresne, and G. Sèze, LMD/IPSL, CNRS, Université Pierre et Marie Curie, F-75252 Paris, France. (chepfer@lmd.polytechnique.fr)

M. Chiriaco, SA/IPSL, CNRS, Université Versailles-Saint Quentin, F-75252 Paris, France.

D. Winker, NASA/LaRC, Hampton, VA 23681, USA.